AGU PUBLICATIONS

Water Resources Research

RESEARCH ARTICLE

10.1002/2015WR017830

# Understanding satellite-based monthly-to-seasonal reservoir outflow estimation as a function of hydrologic controls AQ15

**Matthew Bonnema[1], Safat Sikder[1], Yabin Miao[1], Xiaodong Chen[1], Faisal Hossain[1], Ismat Ara Pervin[2], S. M. Mahbubur Rahman[2], and Hyongki Lee[3]** AQ14

[1]Department of Civil and Environmental Engineering, University of Washington, Seattle, Washington, USA, [2]Water Resources and Planning Division, Institute of Water Modeling, Dhaka, Bangladesh, [3]Department of Civil and Environmental Engineering, University of Houston, Houston, Texas, USA

**Key Points:**
- Mass balance can be used to estimate reservoir outflow
- Snowpack-dominated reservoirs require process-based models
- Joint use of satellite precipitation and water heights can provide outflow

**Correspondence to:**
F. Hossain,
fhossain@uw.edu

**Citation:**
Bonnema, M., S. Sikder, Y. Miao, X. Chen, F. Hossain, I. Ara Pervin, S. M. Mahbubur Rahman, and H. Lee (2016), Understanding satellite-based monthly-to-seasonal reservoir outflow estimation as a function of hydrologic controls, *Water Resour. Res.*, *52*, doi:10.1002/2015WR017830. AQ15

Received 13 JUL 2015
Accepted 30 MAR 2016
Accepted article online 4 APR 2016



**Abstract** Growing population and increased demand for water is causing an increase in dam and reservoir construction in developing nations. When rivers cross international boundaries, the downstream stakeholders often have little knowledge of upstream reservoir operation practices. Satellite remote sensing in the form of radar altimetry and multisensor precipitation products can be used as a practical way to provide downstream stakeholders with the fundamentally elusive upstream information on reservoir outflow needed to make important and proactive water management decisions. This study uses a mass balance approach of three hydrologic controls to estimate reservoir outflow from satellite data at monthly and annual time scales: precipitation-induced inflow, evaporation, and reservoir storage change. Furthermore, this study explores the importance of each of these hydrologic controls to the accuracy of outflow estimation. The hydrologic controls found to be unimportant could potentially be neglected from similar future studies. Two reservoirs were examined in contrasting regions of the world, the Hungry Horse Reservoir in a mountainous region in northwest U.S. and the Kaptai Reservoir in a low-lying, forested region of Bangladesh. It was found that this mass balance method estimated the annual outflow of both reservoirs with reasonable skill. The estimation of monthly outflow from both reservoirs was however less accurate. The Kaptai basin exhibited a shift in basin behavior resulting in variable accuracy across the 9 year study period. Monthly outflow estimation from Hungry Horse Reservoir was compounded by snow accumulation and melt processes, reflected by relatively low accuracy in summer and fall, when snow processes control runoff. Furthermore, it was found that the important hydrologic controls for reservoir outflow estimation at the monthly time scale differs between the two reservoirs, with precipitation-induced inflow being the most important control for the Kaptai Reservoir and storage change being the most important for Hungry Horse Reservoir.



## 1. Introduction

With the global population climbing toward 8 billion, the demand for basic human needs, like food, water, and electricity, is also increasing, causing a strain on the world's water resources. A changing climate also threatens the natural supply of water [*Vörösmarty and Sahagian*, 2000]. AQ1 When demand for water exceeds the natural supply, one of the more common human responses is to impose controls on a natural source of water in order to deliver the water where and when it is needed the most. A widely used form of water control, which provides water in such a regulated manner, is damming a river to create an artificial reservoir.

Dam construction in the developing world is currently on the rise. At least 3700 major dams are either under construction now or planned for construction in the future in the hydropower sector alone, with a majority of these located in developing nations [*Zarfl et al.*, 2014]. The need for dams in these regions is driven by high population growth, need for rapid development, and an increase in urbanization, which in turn strains the local resources. Dams and reservoirs can provide water supply and electricity to help meet these needs. Unfortunately, for downstream stakeholders, upstream dams heavily modify river flows making prediction of flows difficult without knowing the operations of these dams. When these rivers cross international boundaries (referred to as Transboundary Rivers) this becomes an even bigger problem for downstream stakeholders, because the dams represent transboundary reservoirs.

AGU Water Resources Research 10.1002/2015WR017830

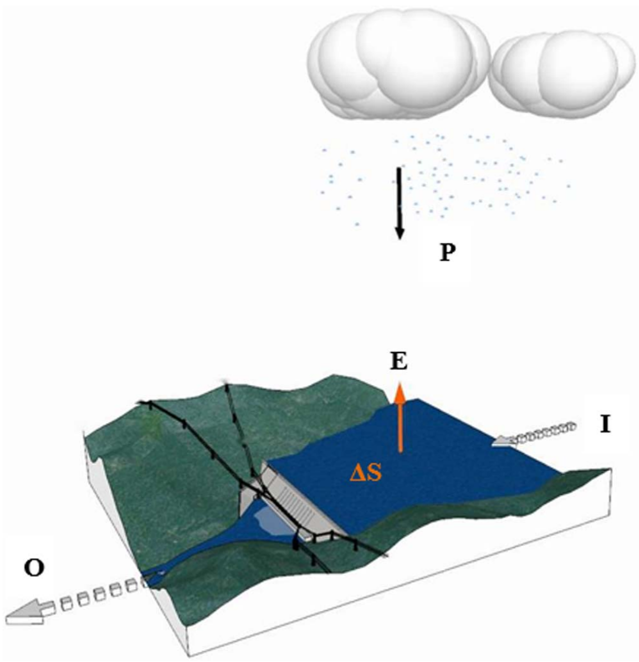


**Figure 1.** Schematic of mass balance between reservoir outflow (O), evaporation (E), changes in reservoir storage (ΔS), and runoff-derived inflow (I) driven by precipitation (P).



Over 260 river systems worldwide have Transboundary Rivers crossing international borders, creating a large set of International River Basins (IRBs) involving 145 countries. IRBs account for more than 40% of the earth's inhabitable surface [*Wolf et al*., 1999]. Historically, water management in IRBs has been difficult, especially in developing nations where ground-based measurement infrastructure is lacking and the ability of nations to jointly manage regional water resources is hindered by poor institutional capacity [*Bakker*, 2009]. This is particularly problematic for downstream nations, as they depend on both upstream hydrologic data and water management practices.

Satellite remote sensing may be used to overcome the challenge of managing water supply downstream of dammed reservoirs in IRBs in the absence of ground-based measurements. Remote sensing has been demonstrated to be useful for a range of water management applications. Recent studies have correlated upstream river height measurements from satellite altimeters with downstream river heights for improved transboundary flood forecasting [*Biancamaria et al*., 2011; *Hossain et al*., 2013, 2014]. Another study developed a framework to incorporate observations from the forthcoming Surface Water and Ocean Topography Mission (SWOT) into the release operations of a dam in the Upper Niger River Basin [*Munier et al*., 2015].

In this study, a combination of satellite altimetry and a satellite precipitation product was used to determine reservoir outflow (Figure 1) through the use of a simple mass balance between hydrologic controls (equation (1)) where reservoir outflow (O) is balanced by changes in reservoir storage (ΔS), precipitation-induced runoff flowing into the reservoir (I), and evaporative losses (E). Due to the revisit period of the satellite observations being longer than a week, the mass balance was resolved on approximately monthly time scales.

$$O = I - E - \Delta S \tag{1}$$

The total change in reservoir storage can be estimated by combining radar altimetry measurements of reservoir surface elevation with remotely sensed reservoir surface area [*Gao*, 2015]. Initially designed for oceanic observations, radar altimetry has been used to accurately measure lake and reservoir elevations since the early 1980s [*Brooks*, 1982; *Mason et al*., 1990; *Birkett*, 1995; *Zhang et al*., 2006; *Lee et al*., 2011]. More recent efforts have combined altimetry with various methods of determining reservoir surface area. *Birkett* [2000] used TOPEX/POSEIDON altimetry measurements with NOAA/AVHRR radiometer images to develop a simultaneous time series of the elevation and water surface extent of Lake Chad. Additionally, *Gao et al*. [2012] used the Moderate Resolution Imaging Spectroradiometer (MODIS) along with satellite radar altimetry to estimate storage changes in 34 global reservoirs. Furthermore, *Salami and Nnadi* [2012] combined altimeter measurements from multiple sources with existing storage-elevation curves and validated their results with a mass balance similar to equation (1) (in their case, outflow was measured with a streamflow gauge and the equation was solved for storage change). A wide array of satellite altimeter missions, both current (JASON-2, AltiKa, Sentinel-1 & 2, Envisat) and future (JASON-3 and Sentinel-3) can be leveraged for the estimation of storage changes [*Lambin et al*., 2010; *Verron et al*., 2015; *Malenovsky et al*., 2012; *Alsdorf et al*., 2007]. Finally, the planned Surface Water and Ocean Topography (SWOT), which will be launched in

AGU Water Resources Research 10.1002/2015WR017830

2020, will provide wide-swath altimetry water height measurements that can inform users on water extent and varying height of the water surface simultaneously.

Precipitation-induced runoff flowing into a reservoir can also be estimated using satellite remote sensing of precipitation. This involves using a satellite precipitation product such as the Tropical Rainfall Measurement Mission (TRMM, now deactivated) or its successor, the Global Precipitation Mission (GPM), to provide an estimate of precipitation over the basin contributing to the reservoir [*Huffman et al*., 2007; *Hou et al*., 2014]. This precipitation can then be fed into a runoff model of appropriate complexity to determine the runoff generated.

As the studies mentioned earlier show, satellite remote sensing of reservoir storage changes is already well addressed. Far fewer studies have attempted to use satellite estimated volume changes to estimate reservoir outflow, which is an important geophysical variable for a wide variety of scientific investigations and applications. *Swenson and Wahr* [2009] used satellite-derived storage changes of a small lake downstream of Lake Victoria to estimate the outflow of Lake Victoria. This approach had high success at the monthly and seasonal time scales, but is specific to Lake Victoria or other systems with a small lake directly downstream of a large reservoir. *Muala et al*. [2014] used altimetry-derived storage changes and in situ inflow measurements to estimate the discharge from Lake Nasser and Rosaries Reservoir in the Nile Basin. They were able to estimate outflow from Rosaries Reservoir to within 18% of observed outflow, while outflow from Lake Nasser was more difficult to predict. It is clear that more investigation into satellite-based reservoir discharge estimation is needed.

Improved knowledge of reservoir outflow provides a greater understanding of the human impacts on the terrestrial water cycle, compared to only reservoir storage. Studies have shown that reservoirs and irrigation water supply withdrawals have decreased annual global discharge into oceans by 2.1% and reservoirs have increased the residence time of surface water by 3 months [*Vörösmarty and Sahagian*, 2000; *Biemans et al*., 2011]. Both of these conclusions have huge implications for downstream ecosystem health, reservoir sedimentation, and water supply. However, a limitation of such global reservoir studies is the absence of observations of reservoir outflow. *Doll et al*. [2009] cites high uncertainties in reservoir operations (which are incidental to reservoir discharges) as a limitation of their global river flow impacts study. Reservoir discharge estimates could be used to refine or localize such studies to more accurately assess regionally specific reservoir impacts.



Additionally, there is value in observing reservoir outflow, rather than reservoir storage change alone from a water management perspective. Knowledge of the amount of water flowing out of an upstream and transboundary reservoir provides downstream stakeholders with a more direct proxy of the amount of water flowing into their region, which has implications for downstream reservoir operations, flood forecasting, and water supply management.

The goals of this study are twofold. First, this study presents a practical method tailored for operationalization of estimating reservoir outflow using the mass balance approach shown in equation (1) and Figure 1, and evaluates this method against observed outflow from two reservoirs in regions with different climates. Second, this study explores the sensitivity of the hydrologic controls included in the mass balance approach for each reservoir and determines which, if any, controls can be reasonably ignored at monthly time scales to enable practical operations.

This study is laid out according to the following: section 2 provides an overview of the two reservoirs considered in this study and the sources of all data used. Section 3 describes the mass balance and the methodology behind computing its various components. Section 4 presents the results for both reservoirs. Section 5 provides a discussion of the results and significant findings. Section 6 concludes with an overview and directions for further study.

## 2. Study Regions and Data

The interaction between hydrologic controls is a function of climate, geography, and size and function of the reservoir. Here the role of climate and geography was explored while keeping function and size relatively constant. As such, this study examined two similarly sized hydropower reservoirs in contrasting climate and geographic settings, Hungry Horse Reservoir and Kaptai Reservoir. Hungry Horse is located in the

AGU Water Resources Research 10.1002/2015WR017830

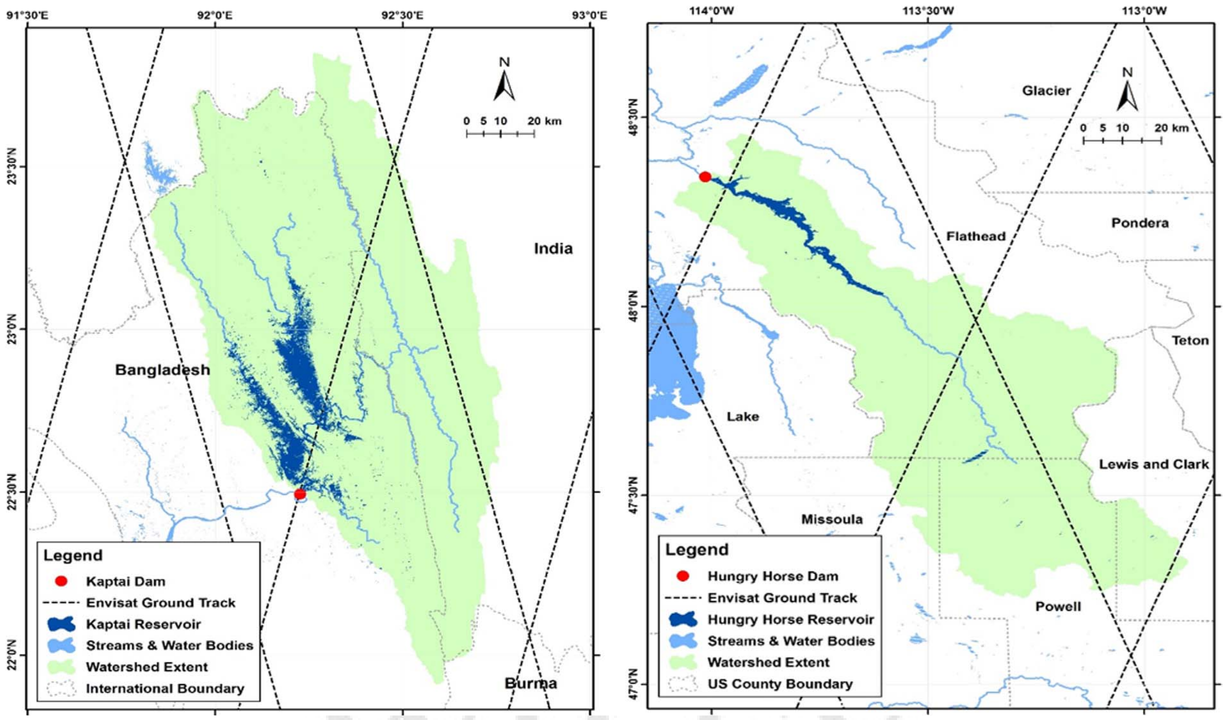


**Figure 2.** Map of the drainage area contributing runoff to the reservoirs as well as the ground track of the Envisat altimeter for (right) Hungry Horse Reservoir and (left) Kaptai Reservoir.



Rocky Mountains of western Montana. It captures water from a 6067 $km^2$ drainage area primarily made up of mountainous forest and has a total water storage capacity of 4.28 $km^3$ [*United States Bureau of Reclamation*, 2013]. Figure 2 shows a map of the watershed draining into the reservoir. There are no dams or other flow regulatory structures upstream of Hungry Horse Dam, but a significant portion of the basin builds up a snowpack in Winter that can act like a natural reservoir until spring snowmelt begins. Constructed from 1948 to 1953, the dam's principal function has been hydroelectric generation with secondary utility as a flood control structure [*United States Bureau of Reclamation*, 2013]. In contrast, Kaptai Reservoir is located on the Karnaphuli River in the Rangamati District of Bangladesh. It should be noted that there are no regulatory structures upstream of Kaptai Reservoir. A map of this reservoir's watershed is also shown in Figure 2. It has a maximum water storage capacity of 6.48 $km^3$ and captures water from a 11,080 $km^2$ area [*Karmakar et al.*, 2009]. Construction of Kaptai Dam finished in 1955 and its primary function to date has been hydropower generation [*Karmakar et al.*, 2009]. It is the only hydropower dam in Bangladesh [*United Nations Environment Programme*, 2004].

All altimeter measurements of both reservoirs were taken by the satellite altimeter Envisat from 21 October 2002 to 4 October 2010 for Hungry Horse Reservoir and 29 October 2002 to 12 October 2010 for Kaptai Reservoir on a 35 day repeat cycle. Envisat (Environmental Satellite) provided 18 Hz retracked data ($\sim$350 m along-track sampling) to estimate water elevation. Interested readers are referred to *Benveniste* [2002] for further details on remote sensing techniques and to *Siddique-E-Akbor et al.* [2011] for an application over inland waters. The locations where the satellite ground tracks cross the reservoirs are shown in Figure 2. Daily precipitation estimates were provided by the 3B42v7 TRMM product [*Huffman et al.*, 2007] for the same time period. This TRMM product has been calibrated against rain gauge observations. These precipitation estimates were conservatively regridded to 0.5° resolution for use in the VIC hydrologic model (section 3.1.2). Digital Elevation Models (DEMs) of each reservoir were obtained from the Shuttle Radar Topography Mission (SRTM), taken from when the reservoirs were at their lowest point observed by the mission [*Farr et al.*, 2007]. Observed outflow for the Hungry Horse Reservoir was measured at USGS streamflow station #12362500, located directly downstream of Hungry Horse Dam. Outflow and river level measurements were available at a gauge station located immediately downstream of the Kaptai Dam and maintained by Bangladesh Water Development Board (BWDB). These data were made available as part of a 5 year Memorandum of Understanding between the Institute of Water Modeling (IWM)-Bangladesh and University of Washington.

AGU Water Resources Research 10.1002/2015WR017830

## 3. Methodology

### 3.1. Mass Balance

In this study, reservoir outflow was calculated as the mass balance of all the inflow and outflow fluxes from the reservoir system, represented by precipitation-induced reservoir inflow (I), changes in reservoir storage ($\Delta S$), evaporation (E), and reservoir outflow (O) outlined in equation (1). It was assumed that groundwater seepage would not be a major factor contributing to reservoir outflow and was ignored.

#### 3.1.1. Reservoir Inflow

Two different hydrologic characterizations of reservoir inflow were used here, the curve number (CN) method and the Variable Infiltration Capacity (VIC) model [*Hawkins et al*., 2002, *Liang et al*., 1994]. Although ease of operation was a key goal of this study, the comparative use of a simple approach like CN and a more complex approach, using a macroscale hydrologic model like VIC, allowed the sensitivity of hydrologic process controls on outflow estimation accuracy to be explored. This is elaborated further in the following sections.

For the application of the CN method, the catchment of each reservoir was delineated from 30 m Digital Elevation Models (DEMs) obtained from the Shuttle Radar Topography Mission (SRTM). The resulting watershed delineations are shown in Figure 2.

Soil type for the Hungry Horse Watershed was obtained from the NRCS Web Soil Survey [*United States Department of Agriculture*, 2009]. Soil data for the Kaptai basin were obtained from the Food and Agriculture Organization of the United Nations Harmonized World Soil Database v 1.2 [*Fischer et al*., 2008]. Land cover of both basins at 1 km resolution was obtained from USGS Land Cover Characterization data [*Loveland et al*., 2000]. From the soil type and land cover data, AMCII (antecedent moisture condition II, referring to average soil moisture) curve numbers for each 1 km grid cell of data were estimated using curve number lookup tables provided by the NRCS Conservation Engineering Division [*Ward and Trimble*, 2004]. The composite curve number (CN) of each basin was calculated as an area weighted average of each curve number. A dynamic curve number approach was used, where the CN alternates among AMC I (dry), AMC II (moderate), and AMC III (wet) conditions, depending on the rainfall (in inches) over the previous 5 days ($P_5$): AQ2

$$CN = \begin{Bmatrix} AMC\ \ I & 0 < P_5 \leq 0.5 \\ AMC\ \ II & 0.5 < P_5 \leq 1.1 \\ AMC\ \ III & P_5 > 1.1 \end{Bmatrix} \tag{2}$$



A similar dynamic CN approach has been used in TRMM-based flood monitoring applications [*Hong et al*., 2007]. The conversion factors between AMC conditions were provided by *Ward and Trimble* [2004]. Once the curve number was known, the daily watershed runoff was estimated from TRMM precipitation data using standard curve number equations (Appendix A).

The VIC hydrologic model is a gridded land surface model (LSM) that characterizes the land cover and soil types and solves energy and mass balance at each grid cell to determine evapotranspiration, interception, surface runoff, subsurface runoff, aerodynamic water fluxes, and snow. VIC models the land surface as flat grid cells. Subgrid heterogeneity in elevation and soil and surface parameters are characterized by statistical distributions. All fluxes and model states are updated at a daily or subdaily time step and each grid cell is simulated independently. Water is only allowed to flow between cells after it has been routed into a channel, and once in the channel, it is not allowed to reenter the soil. The ARNO recession curve is used to characterize the soil moisture balance and the base flow of the lowest soil layer [*Todini*, 1996]. The generation of runoff is determined by the soil saturation excess, calculated by the Xinanjing variable infiltration curve [*Zhao et al*., 1980]. The Penman-Monteith equation is employed to calculate the evapotranspiration [*Shuttleworth*, 1993]. Snow pack is modeled in a two-layer approach, with the upper layer solved separately in the energy balance [*Andreadis et al*., 2009]. The routing model is based on the model described in *Lohmann et al*. [1996, 1998]. Interested readers are referred to *Liang et al*. [1994] for a more detailed description of VIC.

The model has since been updated to model additional processes to improve its performance in a wide range of basins. Of particular importance to this study is the inclusion of frozen soil parameterizations [*Cherkauer and Lettenmaier*, 1999] and snow accumulation and ablation algorithms and updates to cold land processes [*Cherkauer et al*., 2003]. *Haddeland et al*. [2006] used VIC to study the effects of irrigation on the Colorado and Mekong River basins, demonstrating that VIC can be applied to both mountainous basins

AGU Water Resources Research 10.1002/2015WR017830

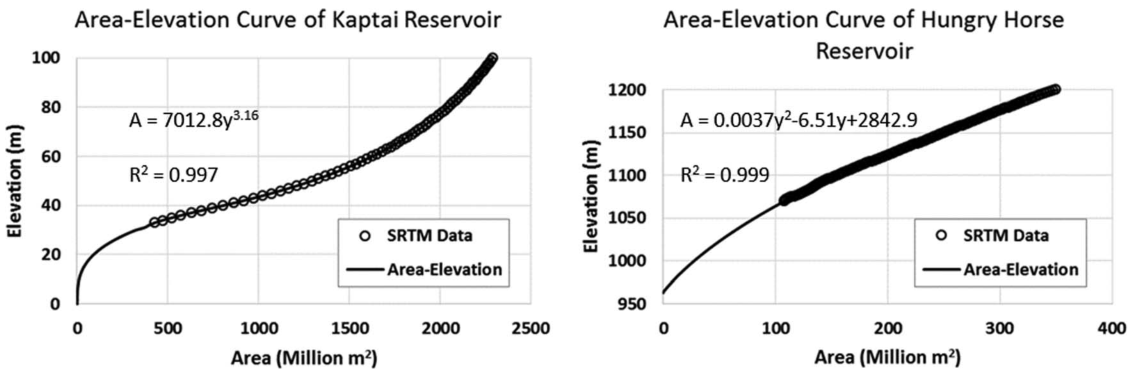


**Figure 3.** Area-Elevation curves for (left) the Kaptai Reservoir and the (right) Hungry Horse Reservoir. Note that the datums of both elevation measurements are the same and that Hungry Horse Reservoir is approximately 1000 m higher in elevation than Kaptai Reservoir.

in the central United States and tropical monsoon basins in Southeast Asia. *Zhu and Lettenmaier* [2007] utilized VIC to study long-term climate trends in the North American monsoon system. *Hamlet and Lettenmaier* [1999a,b] studied climate change and ENSO effects on the snow-dominated Columbia River Basin using a VIC hydrologic model. An important limitation of VIC is its inability to model groundwater. *Wenger et al.* [2010] reports high errors from VIC modeling in basins with strong groundwater influences.

Here a modified 0.5° resolution VIC model with a daily time step, based on the one used in *Zhou et al.* [2015] to study reservoir contributions to global surface water storage variations, was used with the Sheffield global meteorological data set as forcing [*Sheffield et al.*, 2006]. The Sheffield data were regridded to 0.5° resolution for use in the model, using a first-order conservative remapping approach. This model was calibrated against streamflow observations around the world [*Zhou et al.*, 2015]. The precipitation component of the Sheffield data set was replaced with TRMM 3B42v7 precipitation data for both the Hungry Horse and Kaptai basins. The routing model employed by this VIC model used 0.5° resolution river network data from *Wu et al*. [2011].



### 3.1.2. Evaporation

A standard energy balance method [*Chow et al.*, 1988] was used to estimate evaporation from both reservoirs (see Appendix). The average evaporation of each calendar day of the year was used in the mass balance (i.e., the evaporation values on 1 January for all years were averaged to find the typical evaporation on 1 January). The required climatological data for the evaporation estimates of Kaptai Reservoir were provided by the NCDC (National Climatic Data Center) station at Rangamati near Kaptai Lake. Daily evaporation was estimated for the time period of the study using climatological data available from 2011 to 2014. For the Hungry Horse Reservoir, daily evaporation was estimated using a historical record of climate data, from 1948 to 1972. This climatic approach was favored over a more localized weather-scale approach, because this study aimed to explore the feasibility for operational applications around the world, requiring minimal input data.

### 3.1.3. Reservoir Storage Change

The storage change of both reservoirs was estimated as follows. First, the relationship between reservoir water surface elevation and surface area was derived from 30 m resolution DEMs provided by SRTM. The SRTM observations used were those taken when the reservoirs were at their lowest (base water surface elevation), so that the largest portion of reservoir bathymetry was observed. Landsat images over the reservoirs were used to get a better understanding of the minimum reservoir extent. This allowed for knowledge of the bathymetry of the reservoir above this base water surface elevation. From this bathymetry, a relationship between water surface elevation and surface area was determined by classifying the elevation data into 1 m elevation bands and calculating the surface area of each band. A power law function was fitted to the lower elevation-area data of each reservoir to provide an estimate of the elevation area relationship below the water surface elevation at the time the SRTM overpassed the region (during 11–21 February 2000). These curves are shown in Figure 3. This allowed for the calculation of storage volume change using only one type of satellite measurement (elevation) instead of two (elevation and surface area).

These storage-elevation curves were then used, along with radar altimeter measurements of water surface elevation, to derive a time series of water storage changes by approximating the volume of water between two elevations as the average area multiplied by the difference in elevation:

AGU Water Resources Research 10.1002/2015WR017830

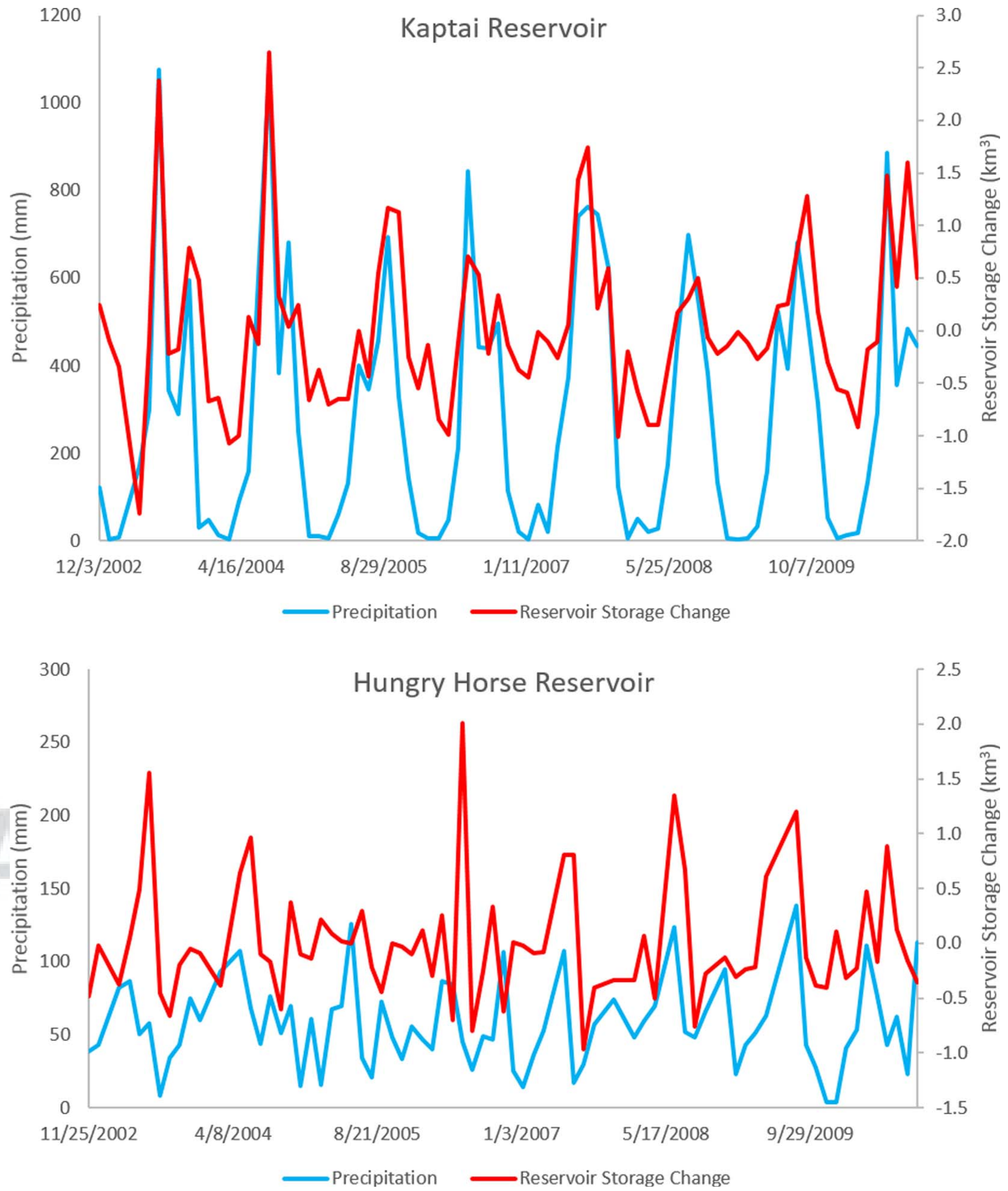


**Figure 4.** Precipitation and reservoir storage change for (top) Kaptai Reservoir and (bottom) Hungry Horse Reservoir. Precipitation is summed over the 35 day period between satellite overpasses. Storage change is the difference between the total amounts of water in the reservoir between two consecutive satellite overpasses, every 35 days.

$$\Delta S = A_{avg.} * \Delta h = \frac{(A_2 + A_1)}{2} * (h_2 - h_1) \quad (3)$$

where

$A_{avg}$ = average of surface area at two elevations;

$\Delta h$ = difference in elevation (between level 1 and 2);

$h_{1,2}$ = elevation measurements at levels 1 and 2, respectively;

$A_{1,2}$ = Surface areas corresponding to $h_1$ and $h_{2;}$

$\Delta S$ = change in reservoir storage between the time when $h_1$ and $h_2$ were observed.

AGU Water Resources Research 10.1002/2015WR017830

These changes in reservoir storage provide the ΔS in the mass balance (equation (1)) for estimating reservoir discharge. A time series of the estimated storage changes for both reservoirs is shown in Figure 4 along with the precipitation into each basin. F4

This approach is similar to the approach used by *Zhang et al*. [2006] to measure water storage in Lake Dongting in China. They reported a correlation coefficient (R) of 0.96 between in situ observations and altimetry-based storage fluctuations. *Salami and Nnadi* [2012] applied a similar technique to Kainji Reservoir in Nigeria and found an $R^2$ of 0.93 between in situ and altimetry-based storage changes.

### 3.2. Hydrologic Controls

The importance of the hydrologic controls (I, E, and ΔS) to the estimation of reservoir outflow was assessed based on the outflow accuracy from different combinations of controls in the mass balance. The combinations explored here were IES, IS, ES, and S. Near monthly (35 day), reservoir outflow was calculated using the mass balance described in section 3.1 for each of these combinations of hydrologic controls. By comparing the accuracy of estimated outflow between each combination, the relative impact each control had on the mass balance was estimated.

### 3.3. Inflow Error Assessment

Of the three hydrologic controls described in section 3.2, the method of estimating inflow into the reservoir using the VIC hydrologic model is considerably more complex than the estimation of evaporation, storage change, or inflow with the curve number method. This study explores how precipitation errors propagate through the VIC model in order to gain a better understanding of the sources of error in the resulting reservoir outflow estimate. Because of the varying availability of precipitation data, the method for exploring inflow errors was different for each basin.

#### 3.3.1. Kaptai Inflow Error Assessment

Daily precipitation from a rain gage in the Kaptai basin, located on Kaptai Reservoir, was compared to daily precipitation from the 0.25° TRMM grid cell containing the gage to understand how accurate TRMM precipitation estimates were, compared to trusted, ground-based precipitation measurements. TRMM precipitation over the Kaptai basin was also compared with the Sheffield global data set precipitation. Then, both TRMM and Sheffield precipitation were used as forcings in the VIC model of the basin. The resulting runoffs (which served as inflow into the reservoir) were also compared, to provide as sense of how error in precipitation propagates through the VIC model.

#### 3.3.2. Hungry Horse Inflow Error Assessment

The TRMM precipitation data were compared to precipitation from the PRISM data set (PRISM Climate Group, Oregon State University, http://prism.oregonstate.edu, created 29 December 2015). The PRISM data were conservatively regridded to match the 0.25° resolution of the TRMM precipitation data. These two precipitation data sets were then used to force the VIC model of the Hungry Horse Basin and the resulting runoffs (inflows into the reservoir) were compared. Because snow processes play an important role in the hydrology of this basin, the snow water equivalent (SWE) outputs from each VIC model run were compared.

## 4. Results

Hydrographs comparing the mass balance estimated outflow for various combinations of hydrologic controls with observed outflow for the Kaptai Reservoir are shown in Figure 5, for both the CN method and the VIC model. Similar comparison hydrographs for the Hungry Horse Reservoir are shown in Figure 5. Outflow is presented as the total volume of water that passed through the reservoir every 35 days between satellite overpasses. The corresponding error statistics are shown in Table 1 for Kaptai Reservoir and Table 2 for Hungry Horse. These statistics are the root-mean-squared error (RMSE), relative root-mean-squared error (RRMSE), relative bias, and the Nash-Sutcliffe model efficiency coefficient (NSE). It should be noted that Winter refers to December, January, and February; Spring refers to March, April, and May; Summer refers to June, July, and August; and Fall refers to September, October, and November. The annual discharge was also estimated for each reservoir for 2003–2009. The years 2002 and 2010 were excluded from this portion of the analysis because the period of study used at monthly time scales does not include the entirety of 2002 or 2010. A comparison between this estimated annual outflow and observed annual outflow is given in Table 3 as a percent difference between estimated and observed outflow. Here negative percent difference indicates that the estimate was an under prediction of the observed. Table 3 also provides RMSE,

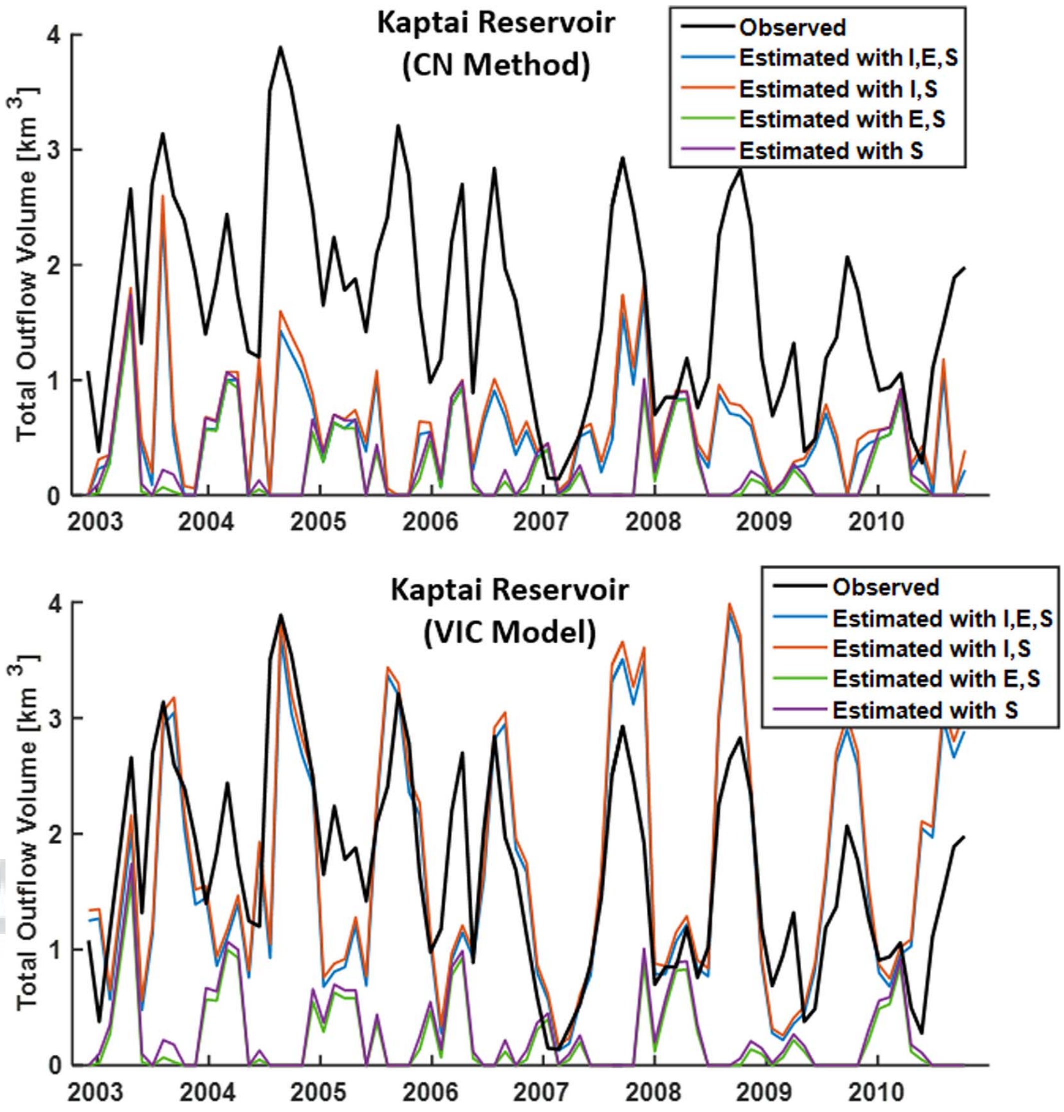


**Figure 5.** Hydrographs comparing Kaptai Reservoir discharge observations to discharge estimates using different components of the mass balance, changes in storage (S), runoff inflow (I), and evaporation (E). The inflow in the top graph uses the CN method while the inflow in the bottom graph uses the VIC model.

RRMSE, relative bias, and NSE for the annual outflow estimates. The annual estimates were examined in conjunction with yearly precipitation totals, but no clear correlation between accuracy and bias of the estimates and precipitation amount was found.

### 4.1. Kaptai Reservoir

Using the CN method to provide inflow, the I, E,S estimated outflow had an overall RRMSE of 83.2% and an NSE of $-1.50$ at the monthly time scale across all seasons. Replacing the inflow estimation method with the VIC model, the I,E,S estimated outflow improved, with an overall RRMSE of 46.8% and an NSE of 0.22. Removing the evaporation component from these monthly estimates slightly increased the accuracy of outflow estimates using CN-derived inflow and slightly decreased the accuracy of outflow estimates using VIC-derived inflow. The two estimates that exclude inflow showed considerably lower accuracy than both inflow methods and large negative biases. Monthly outflow predictions made using CN-derived inflow during the dry season (Winter and Spring) exhibited small gains in accuracy over predictions made without inflow. Predictions utilizing VIC inflow showed larger gains in accuracy in the Winter months. The I,S outflow estimate using VIC was the most accurate dry season estimate, with the I,E,S estimate using VIC performing only

AGU Water Resources Research 10.1002/2015WR017830

**Table 1.** Error Statistics for Kaptai Reservoir Discharge Estimations Including Different Hydrologic Controls, Changes in Storage (S), Runoff Inflow (I), and Evaporation (E)[a]

| | | I,S,E (CN) | I,S (CN) | I,S,E (VIC) | I,S (VIC) | E,S | S |
|---|---|---|---|---|---|---|---|
| Overall | RMSE (km$^3$) | 1.39 | 1.32 | 0.78 | 0.80 | 1.72 | 1.70 |
| | RRMSE (%) | 83.2 | 79.3 | 46.8 | 47.8 | 103.4 | 101.7 |
| | Relative Bias (%) | −67.89 | −63.20 | −1.15 | 6.2 | −86.78 | −84.13 |
| | NSE | −1.50 | −1.27 | 0.22 | 0.19 | −2.87 | −2.74 |
| Winter | RMSE (km$^3$) | 0.89 | 0.83 | 0.60 | 0.57 | 0.94 | 0.88 |
| | RRMSE (%) | 82.2 | 76.9 | 54.4 | 52.0 | 86.8 | 81.4 |
| | Relative Bias (%) | −68.31 | −62.23 | −20.55 | −14.60 | −72.96 | −66.98 |
| | NSE | −1.29 | −1.01 | 0.03 | 0.09 | −1.56 | −1.25 |
| Spring | RMSE (km$^3$) | 0.90 | 0.85 | 0.82 | 0.80 | 0.98 | 0.93 |
| | RRMSE (%) | 65.5 | 61.5 | 59.7 | 57.2 | 70.9 | 67.3 |
| | Relative Bias (%) | −55.46 | −50.36 | −26.89 | −22.04 | −63.49 | −58.83 |
| | NSE | −0.49 | −0.32 | −0.20 | −0.13 | −0.75 | −0.58 |
| Summer | RMSE (km$^3$) | 1.59 | 1.52 | 0.93 | 0.97 | 2.15 | 2.13 |
| | RRMSE (%) | 80.6 | 77.0 | 46.5 | 49.0 | 108.6 | 107.6 |
| | Relative Bias (%) | −66.37 | −61.86 | 8.21 | 14.29 | −98.46 | −97.46 |
| | NSE | −2.10 | −1.83 | −0.05 | −0.14 | −4.63 | −4.53 |
| Fall | RMSE (km$^3$) | 1.91 | 1.85 | 0.72 | 0.85 | 2.52 | 2.50 |
| | RRMSE (%) | 81.5 | 76.0 | 30.9 | 35.0 | 103.8 | 102.9 |
| | Relative Bias (%) | −76.27 | −68.90 | 16.99 | 25.07 | −99.52 | −98.67 |
| | NSE | −9.34 | −8.53 | −0.48 | −0.83 | −14.98 | −14.69 |

[a]Statistics are broken down by season (Spring: March-April-May, Summer: June-July-August, Fall: September-October-November, Winter: December-January-February).

**Table 2.** Error Statistics for Hungry Horse Reservoir Discharge Estimations, Including Different Hydrologic Controls, Broken Down by Season[a]

| | | I,S,E (CN) | I,S (CN) | I,S,E (VIC) | I,S (VIC) | E,S | S |
|---|---|---|---|---|---|---|---|
| Overall | RMSE (km$^3$) | 0.27 | 0.27 | 0.20 | 0.20 | 0.27 | 0.27 |
| | RRMSE (%) | 86.0 | 86.4 | 62.7 | 64.3 | 86.4 | 86.8 |
| | Relative Bias (%) | −28.07 | −24.43 | 15.23 | 17.68 | −28.58 | −24.69 |
| | NSE | −1.02 | −1.04 | −0.08 | −0.13 | −1.05 | −1.06 |
| Winter | RMSE (km$^3$) | 0.10 | 0.10 | 0.09 | 0.09 | 0.11 | 0.11 |
| | RRMSE (%) | 44.0 | 42.1 | 39.8 | 39.2 | 48.6 | 46.7 |
| | Relative Bias (%) | −21.75 | −20.04 | 8.83 | 10.80 | −21.96 | −20.09 |
| | NSE | 0.14 | 0.22 | 0.30 | 0.32 | −0.05 | 0.03 |
| Spring | RMSE (km$^3$) | 0.27 | 0.27 | 0.20 | 0.20 | 0.27 | 0.27 |
| | RRMSE (%) | 88.7 | 88.6 | 67.9 | 66.8 | 88.6 | 88.5 |
| | Relative Bias (%) | −40.87 | −38.98 | −7.47 | −3.74 | −42.61 | −40.72 |
| | NSE | −0.30 | −0.30 | 0.24 | 0.26 | −0.30 | −0.29 |
| Summer | RMSE (km$^3$) | 0.42 | 0.42 | 0.23 | 0.23 | 0.42 | 0.42 |
| | RRMSE (%) | 88.9 | 89.0 | 48.1 | 48.4 | 89.2 | 89.3 |
| | Relative Bias (%) | −50.90 | −46.58 | 4.11 | 2.34 | −51.72 | −47.41 |
| | NSE | −5.22 | −5.24 | −0.82 | −0.85 | −5.27 | −5.28 |
| Fall | RMSE (km$^3$) | 0.16 | 0.17 | 0.22 | 0.24 | 0.16 | 0.17 |
| | RRMSE (%) | 66.5 | 70.4 | 92.1 | 99.7 | 66.1 | 70.0 |
| | Relative Bias (%) | 26.20 | 32.22 | 69.17 | 78.72 | 27.50 | 34.65 |
| | NSE | −1.67 | −1.99 | −4.12 | −5.00 | −1.64 | −1.96 |

[a]Spring: March-April-May, Summer: June-July-August, Fall: September-October-November, and Winter: December-January-February.

**Table 3.** Percent Difference Between Observed and Estimated Annual Total Flows[a]

| | Percent Difference by Year (%) | | | | | | | Overall Error | | | |
|---|---|---|---|---|---|---|---|---|---|---|---|
| Year | 2003 | 2004 | 2005 | 2006 | 2007 | 2008 | 2009 | RMSE (km$^3$) | RRMSE (%) | Rel. Bias (%) | NSE |
| Kaptai (VIC) | −17.8 | −25.9 | −13.9 | −13.5 | 28.0 | 15.8 | 16.0 | 3.66 | 20.4 | −5.98 | 0.30 |
| Kaptai (CN) | −68.5 | −67.1 | −79.1 | −68.1 | −51.2 | −63.0 | −74.4 | 12.73 | 71.1 | −68.01 | −7.47 |
| Hungry Horse (VIC) | 29.9 | 22.7 | −7.7 | 48.0 | −15.0 | 5.2 | 23.6 | 0.75 | 26.4 | 14.99 | −1.63 |
| Hungry Horse (CN) | −12.3 | −31.6 | −60.4 | 19.7 | −29.4 | −35.8 | −19.1 | 0.98 | 34.2 | −23.75 | −3.41 |

[a]A negative percent difference represents an underprediction in the estimate.

slightly worse. Including CN-based inflow in the mass balance resulted in larger increases in accuracy in the wet season than the dry season. Replacing CN-derived inflow with VIC modeled inflow provided another significant improvement in outflow estimation accuracy, with the lowest seasonal RRMSE occurring in the Fall. Similar to the dry season, the E,S and S outflow estimates were considerably less accurate compared to other estimates in the Fall. The NSE of the VIC I,E,S outflow estimation for each season ranged from 0.03 to −0.48, while the NSE for the overall estimate was 0.22. This indicates that the mass balance estimate utilizing VIC modeled inflow was a better predictor of monthly outflow than the average monthly outflow from 2002 to 2010 would be, while seasonal average outflow would be a more accurate predictor of monthly outflow than the mass balance estimate.

The difference between outflow estimate accuracy of the two inflow methods was smaller in the dry season (Winter and Spring), with less than 10% RRMSE differences in the spring. However, in the dry season, CN-driven outflow estimates more closely match outflow estimates derived from storage change only, with differences in RRMSE around 5%. This trend can be seen in the hydrograph in Figure 5. Conversely, wet season CN-driven outflow estimates showed a significant increase in accuracy over estimates excluding the inflow component, as shown by decreases in RRMSE between 28.0% and 20.6% during this period. VIC model-driven outflow estimates exhibit even higher accuracy improvements over the CN-driven estimate in the wet season than in the dry season, with RRMSE differences as high as 50.6%. CN-driven outflow estimates exhibited large negative relative biases across all seasons, which is reflected in the hydrograph (Figure 4).

Comparison between observed and estimated total outflow using the VIC model at annual time scales reveals a shift from underestimation to overestimation of annual outflow between 2006 and 2007. Pre-2006 outflow estimates match the wet season peaks, but underestimate dry season low flows. In contrast, post-2006 outflow estimates over-predict peak wet season discharge, but better capture dry season low flows. Further exploration of this trend is provided in section 5. This shift is reflected by the low overall relative bias, where the overestimates compensated for the underestimates. The percent difference between estimated and observed annual outflow ranged from 13.9% to 28.0% in magnitude with no clear trend over time. With an RRMSE of 20.4% and NSE of 0.30, the mass balance performed with higher accuracy at the annual time scale than the monthly time scale at this reservoir.



The CN-driven annual outflow estimates did not follow this pattern and the percent difference between observed and estimated outflow remained between −51.2% and −79.1%, with no clear trend over time. An RRMSE of 71.1% indicates that the mass balance using CN inflow estimated annual outflow with more skill than monthly outflow. However, it performed significantly worse than the mass balance using the VIC model inflow as illustrated by the drastic difference between RRMSE and NSE of the two annual outflow estimates.

### 4.2. Hungry Horse Reservoir

Estimations of outflow from the Hungry Horse Reservoir resulted in instances of outflow considerably lower than expected. These instances occurred fewer than once a year on average. It is clear that a hydrologic process was not properly represented, even by the VIC model, however the exact reason for these errors is unclear. Given the small number of these errors in estimates made using VIC model inflow, a minimum flow threshold was implemented here to correct for these errors. This threshold was provided by a State of Montana operation constraints report and set at 300 cfs (to meet environmental flow requirements downstream), which corresponds to 0.026 km$^3$ in a 35 day period [*State of Montana*, 2011]. Outflow estimates that violated this limit were instead taken as the average of the previous and subsequent outflow estimates. Outflow estimates generated with CN-derived inflow or generated without considering inflow experienced more frequent errors of this nature, with multiple erroneous outflow estimates occurring in subsequent time steps. In these instances, the averaging correction could not be applied and the discharge values were set at 0.25 km$^3$. This corrective approach requires reservoir-specific and river-specific data and thus might not be applicable to other reservoirs. However, a minimum threshold of no flow can be applied to all reservoirs if negative outflow becomes an issue.

Outflow estimates that used CN-derived inflow were nearly identical to estimates that excluded the inflow component across all seasons. This is reflected by similar error statistics between estimates with and without the CN-derived inflow component, and can be clearly seen in Figure 6. From Table 2, the I,E,S estimated outflow with inflow derived from the VIC model was most accurate overall with an RRMSE of 62.7%, followed closely by the I,S estimates with 64.3%. Outflow estimates that utilized CN-derived inflow and those that excluded inflow were less accurate, ranging from 86.0% and 86.8% RRMSE. Estimates that included VIC

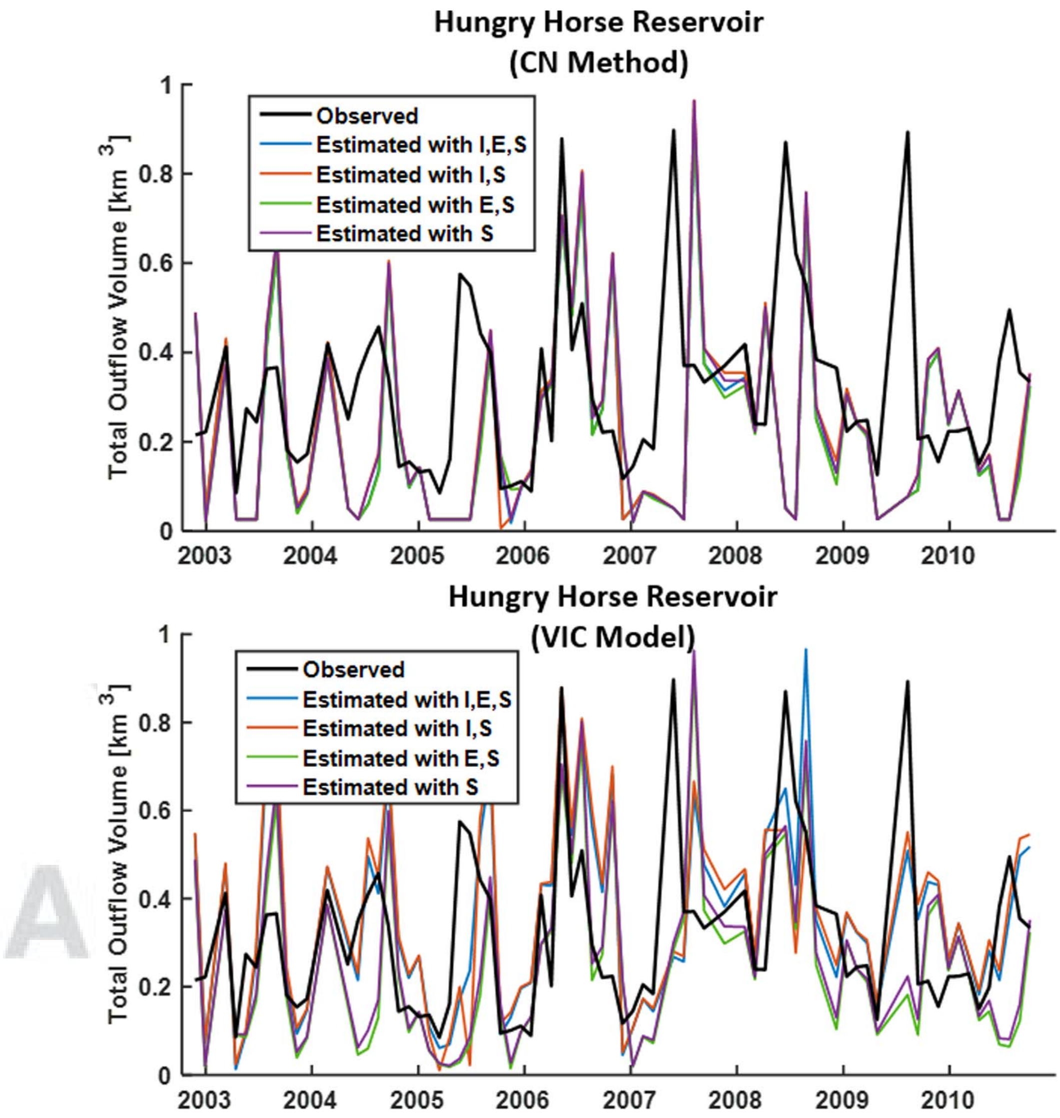


**Figure 6.** Hydrographs comparing Hungry Horse Reservoir discharge observations to discharge estimates using different components of the mass balance, changes in storage (S), runoff inflow (I), and evaporation (E). The inflow in the top graph uses the CN method while the inflow in the bottom graph uses the VIC model.

modeled inflow tended to overpredict discharge as shown by positive relative bias. Estimates utilizing CN-derived inflow or lacking the inflow component exhibited negative relative bias with higher magnitude.

Winter outflow estimation was considerably more accurate. Outflow estimates using CN-derived inflow showed small gains in accuracy over estimates that excluded inflow. Outflow estimates utilizing VIC modeled inflow were the most accurate here with RRMSEs of 39.8% and 39.2% for I,E,S and I,E estimates, respectively. Spring discharge estimates provided RRMSE similar to the overall RRMSE for all mass balance component combinations, but with lower relative bias. The lowest relative bias (2.34%) occurred in the summer with VIC providing inflow. Summer RRMSE for this estimate was 48.1%. In contrast to the other seasons, fall estimates without inflow exhibited higher accuracy than estimates including inflow, with an RRMSE of 66.4% for the E,S estimate and a relative bias of 25.25%. Based on the overall NSE, the mass balance estimates were not better predictors of monthly discharge than the 2002–2010 mean flow would be. Seasonally, the mass balance predicted flows more accurately than the seasonal mean outflow in the Winter and Spring, and less accurately in the Summer and Fall.

With an RRMSE of 34.2%, the mass balance including CN inflow estimated annual reservoir outflow more skillfully than monthly inflow. Annual outflow estimates that used CN-derived inflow consistently

**Table 4.** Comparison Between TRMM Precipitation and the Kaptai Reservoir Rainfall Gage as Well as Between TRMM and the Sheffield Global Data Set Precipitation

| | Overall | DJF | MAM | JJA | SON |
|---|---|---|---|---|---|
| *TRMM and Kaptai Reservoir Rainfall Gage* | | | | | |
| RMSE (mm/d) | 15.39 | 1.93 | 6.65 | 25.4 | 15.87 |
| Hit bias (mm/d) | −3.39 | −0.11 | −0.46 | −8.55 | −4.28 |
| Missed precipitation (%) | 6.87 | 0.56 | 1.31 | 18.3 | 7.14 |
| False precipitation (%) | 15.94 | 3.33 | 22.88 | 23.08 | 15.93 |
| *TRMM and Sheffield* | | | | | |
| RMSE (mm/d) | 9.78 | 4.26 | 8.53 | 13.13 | 10.87 |
| Hit bias (mm/d) | 1.86 | −0.51 | 0.70 | 3.78 | 0.86 |
| Missed precipitation (%) | 6.47 | 8.43 | 7.95 | 3.27 | 6.26 |
| False precipitation (%) | 35.87 | 12.40 | 30.41 | 62.45 | 37.74 |

underestimated observed annual outflow (represented by negative percent difference), with the exception of 2006. In contrast, the mass balance consistently overestimated annual outflow (represented by positive percent difference) when utilizing the VIC model inflow component, with underprediction only occurring in 2005 and 2007. Percent differences between observed and estimated annual outflow utilizing VIC inflow ranged in magnitude from 5.2% in 2007 to 48% in 2006. There is no clear trend in the accuracy of the discharge estimates over time. An RRMSE of 26.4% suggests that the mass balance estimated discharge with higher skill at the annual time scale than the monthly time scale. However, an NSE of −1.63 indicates that the mass balance is a worse predictor of annual outflow than the 2003–2009 average annual outflow.

### 4.3. Inflow Error Assessment Results

Table 4 shows the RMSE, hit bias, probability of missed precipitation, and probability of false precipitation for the comparison between TRMM precipitation and Sheffield precipitation and between TRMM and the rainfall gage station at Kaptai Reservoir. Interested readers are referred to *Tian and Peters-Lidard* [2010] for more information regarding hit bias, missed precipitation, and false precipitation, and to *Gebregiorgis et al*. [2012] for more information on how these errors propagate. These statistics are shown for the entire study period as well was for consecutive 3 month seasons (i.e., precipitation errors from every December, January, and February were considered for the statistics listed under "DJF"). The pattern in RMSE is the same for both comparisons, with the lowest occurring in DJF and the highest in JJA. TRMM appears negatively biased when compared to the gage, but positively biased when compared to Sheffield. Additionally, the season distribution of missed precipitation is different, but the overall missed precipitation for both comparisons is similar. The rainfall gage comparison indicates that TRMM falsely identifies precipitation over twice as much as the Sheffield comparison. Some differences between these two comparisons are expected however, because the comparison with the rainfall gage only takes into account one TRMM grid cell, while the Sheffield comparison examines the entire domain. T4



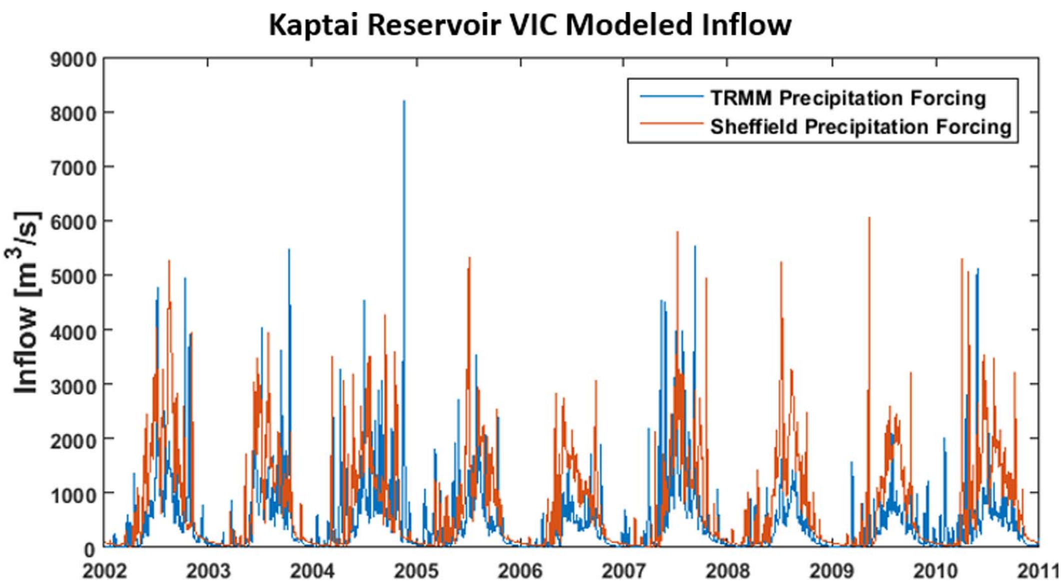


**Figure 7.** Comparison between daily Kaptai Reservoir inflow generated by the VIC model forced by TRMM and Sheffield precipitation data.

**Table 5.** Comparison Between Daily TRMM and PRISM Precipitation From 2002 to 2010 Over the Hungry Horse Basin

| | Overall | DJF | MAM | JJA | SON |
|---|---|---|---|---|---|
| RMSE (mm/d) | 4.25 | 4.67 | 4.15 | 3.85 | 4.30 |
| Hit bias (mm/d) | −1.58 | −2.17 | −1.65 | −0.97 | −1.55 |
| Missed precipitation (%) | 31.2 | 50.2 | 27.8 | 14.8 | 32.2 |
| False precipitation (%) | 11.6 | 3.0 | 19.0 | 16.5 | 7.8 |

The resulting daily inflow generated from the VIC model forced with TRMM precipitation is compared to the inflow generated from the VIC model forced with Sheffield precipitation in Figure 7. From this graph, it can be seen that inflow produced with TRMM and Sheffield precipitation follow similar seasonal patterns with similar magnitude in peak flows. However, the timing of these peak flows appears to be different in many cases. This leads to a high error between the two inflows, but a low bias. When these daily inflows are aggregated into monthly inflows, these timing errors are eliminated and result in an RRMSE between the two monthly inflows of less than 10%.

Table 5 shows the RMSE, hit bias, probability of missed precipitation, and probability of false precipitation for the comparison between TRMM precipitation and PRISM precipitation over the Hungry Horse basin. TRMM has the highest RMSE, hit bias, and missed precipitation in the DJF when most of the precipitation is

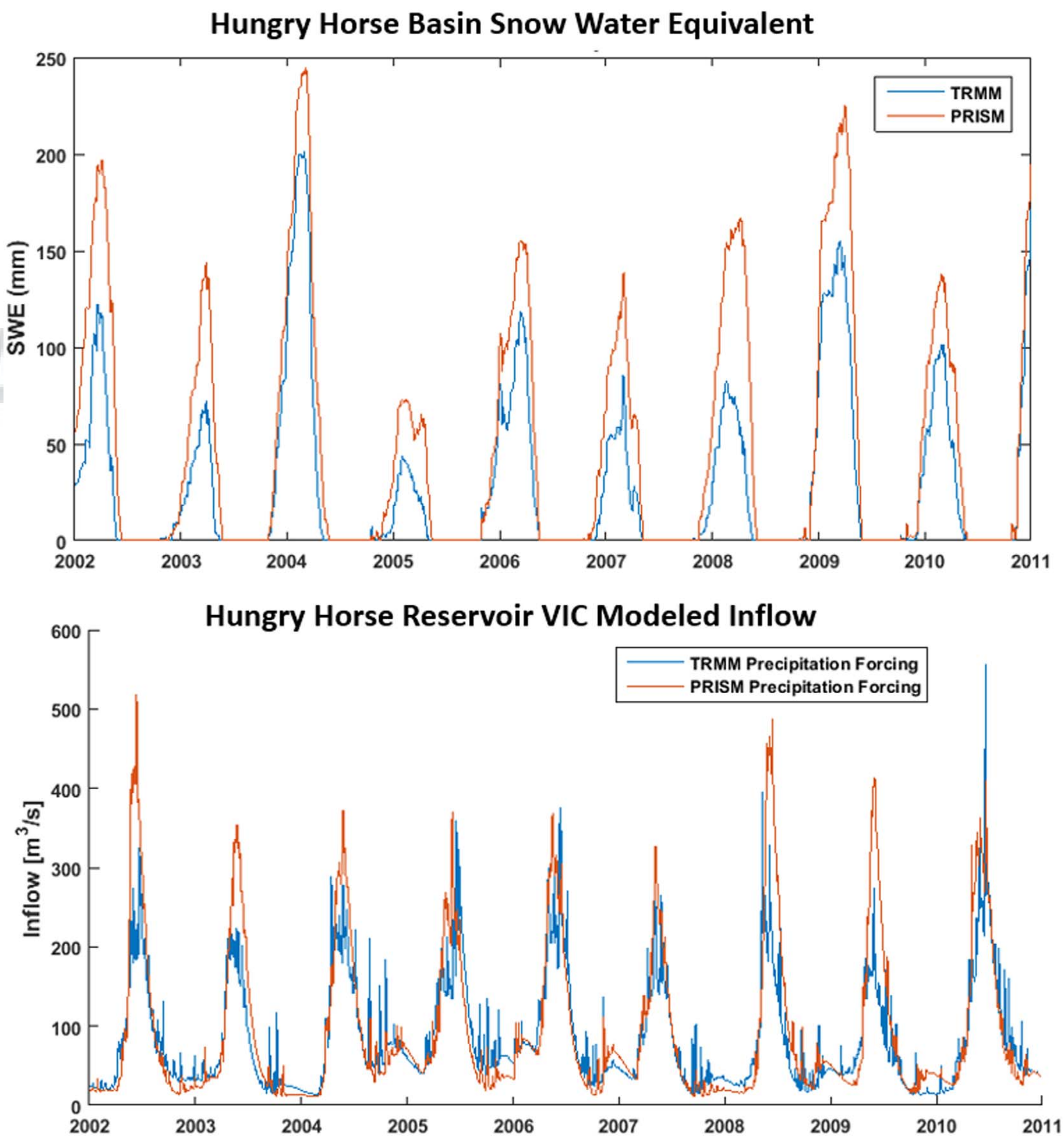


**Figure 8.** Comparison between VIC model outputs generated using TRMM and PRISM precipitation as forcings, (top) average snow water equivelent and (bottom) inflow into the Hungry Horse Reservoir.

AGU Water Resources Research 10.1002/2015WR017830

snow. TRMM is also negatively biased across all seasons, indicating an underrepresentation of precipitation in this basin. Figure 8 shows the daily basin average snow water equivalent (SWE) in the basin generated using the VIC model with both sets of precipitation forcings (TRMM and PRISM). Figure 8 also shows the resulting inflow generated by the VIC model using both precipitation forcings. From the SWE comparison, it is clear that TRMM precipitation causes consistently lower SWE than PRISM. This leads to the consistently lower spring and summer peak inflows shown in the inflow comparison graph.

F8

## 5. Discussion

The mass balance approach utilizing CN-derived inflow demonstrated small gains in monthly Kaptai Reservoir outflow estimation over mass balance approaches that excluded inflow. Conversely, the mass balance approach utilizing VIC modeled inflow yielded fairly accurate monthly outflow estimates. The outflow estimation accuracy improvements achieved by utilizing the VIC model to derive inflow over the CN method suggest that improved modeling of the hydrologic inflow processes led to more accurate outflow estimates. Furthermore, examination of the seasonal differences in monthly outflow estimation revealed higher accuracies in the wet season than the dry season. This indicates that the mass balance and VIC inflow model better represent the hydrological processes during the wet season. A seasonal shift in the relative bias from negative (underestimations) in the dry season to positive (overestimation) in the wet season is observed for VIC inflow-based estimations. However, the hydrograph in Figure 5 reveals that overestimation of wet season outflow only occurred from 2007 to 2010. During 2002–2006, wet season outflow estimates appear to match observed outflow. Similarly, dry season underestimation occurred primarily in 2002–2006, while dry season estimates in 2007–2010 match observations more closely. This indicates a shift in the conditions of this basin that caused outflow estimates to increase in all seasons. One possible explanation is a change in basin characteristics through land cover or land use changes, such as an increase in vegetation, which would cause a larger portion of precipitation to be intercepted leading to less runoff flowing into the reservoir than predicted. This highlights the vulnerability of this method to changing basin conditions, as any changes would have to be accounted for in the runoff model. Estimates that utilized CN inflow did not appear to follow this pattern, indicating that the process that caused this shift is poorly represented by the curve number method.



Comparison between observed outflow and outflow estimated using different components of the mass balance showed that the accuracy of the outflow estimate was highly variable and depended on which hydrologic controls were considered. For the Kaptai Reservoir, the two most accurate combinations of controls were I,E,S (inflow, evaporation, and storage change) and I,S (inflow and storage change), when the VIC model was used to provide inflow. The difference in accuracy between these two cases was relatively small. This, in conjunction with the high error in estimated outflow in both cases where inflow was not included, indicated that precipitation-induced inflow is the most important hydrologic control to consider for this reservoir, which is consistent with the region's high precipitation. This is reflected by the significant accuracy improvements achieved utilizing a more complex, process-based approach (VIC) over a simpler, more empirical approach (CN). This is further supported by the size of the reservoir relative to the inflow. The Kaptai Reservoir has the capacity to store only 33% of the average annual runoff of this time period. This indicates that inflow and outflow should be considerably larger than storage change in this reservoir. However, storage change was also an important control to consider, particularly during periods of low precipitation. While including evaporation in the mass balance resulted in an overall lower relative bias, the effects on outflow estimation accuracy were minimal. At this time, it is unclear if evaporation is an insignificant control for this reservoir, or if the climatologic evaporation approach used here is insufficient and a more localized, weather-based approach is needed.

As a source of error for the Kaptai Reservoir, the precipitation input likely had little effect. The error and bias present when comparing TRMM precipitation to Sheffield precipitation were reduced when these precipitation data sets were used as forcings in the VIC model, and were further reduced when the resulting runoff (inflow into the reservoir) was aggregated over monthly time scales.

The mass balance approach for the Hungry Horse Reservoir provided less accurate monthly outflow overall. However, Winter outflows from Hungry Horse were estimated with a significant degree of accuracy and compelling NSE, when the VIC model provided the inflow component. Utilizing the CN method to provide inflow did little to improve accuracy over simply excluding inflow. This suggests that the VIC model captures one or more hydrological processes that control the runoff in this basin that are otherwise poorly represented by the CN method. This important process is likely snow accumulation/melt, characteristic of high-elevation basins such as the Hungry Horse basin. The VIC model, through energy balance, can represent the timing and magnitude of snow accumulation/melt while the CN method has no capacity to represent snow processes. Winter is the only season where inflow is typically not effected by snowmelt, as a majority of the basin remains below freezing throughout the Winter. The relatively lower accuracy during the other seasons could be caused by difficulties in estimating the quantity and timing of snow accumulation/melt. This is supported by the findings of the inflow error analysis, where differences in Winter SWE (resulting from two different precipitation forcings) caused similar differences in spring and summer runoff. Including inflow in the mass balance provided an increase in outflow estimation accuracy, indicating that inflow is an important hydrologic control in this basin. However, the magnitude of the storage change was considerably larger relative to inflow. This is supported by the Hungry Horse Reservoir's size relative to annual runoff. The reservoir has the capacity to store 144% of the average annual flow during the study period. This suggests storage change is the most important hydrologic control in this basin. Representing inflow properly was also important in generating accurate outflow estimates as demonstrated by the differences between the I,E,S (VIC) estimate, the E,S estimate, and the I,E,S (CN) estimate. However, excluding inflow improved the accuracy in the fall. A possible source of this anomaly is an overestimation of inflow and runoff during this time as suggested by the high relative bias associated with the I,E,S (VIC) estimate. The partition between the forms of precipitation (rain or snow) into the basin in the fall is highly sensitive to the climate. It is possible that the model forcing does not accurately reflect the conditions at the higher elevation points in the basin, causing the VIC model to erroneously treat fall snow precipitation as rain. Furthermore, slight inaccuracies in the VIC model's partitioning between snow accumulation and melt would have high impacts on the resulting inflow. This could lead to the overestimated Fall outflows generated with inflow included in the mass balance.

Unlike the Kaptai Reservoir, outflow estimation for the Hungry Horse Reservoir was significantly impacted by errors in the TRMM precipitation input. The negative bias of TRMM precipitation compared to PRISM precipitation, particularly in the Winter, propagated through the VIC model and resulted in negatively biased inflow. A similar negative bias is seen in spring outflow estimation, when runoff is at a peak due to snowmelt. Additionally, groundwater effects in the basin, which are not modeled by VIC, could significantly affect inflow.

Annual outflow totals of both reservoirs were estimated more accurately than monthly outflow, indicating that the mass balance approach for annual estimations has more value than for monthly estimations. These annual estimates once again illustrate which hydrologic controls were important for each basin. The difference in accuracy between Kaptai Reservoir annual outflow estimated from VIC inflow and CN inflow was extreme, identifying inflow as a key component of outflow estimation in this basin. In contrast, the difference in accuracy between Hungry Horse Reservoir annual outflow estimated from VIC inflow and CN inflow was less pronounced. This signifies that while inflow is a significant hydrologic control, it is not the dominant control. However, the low NSE for the annual Hungry Horse outflow indicates that even at yearly time scales, some source of error is hindering the mass balance's effectiveness. This could be errors in TRMM precipitation propagating through the VIC model, or high connectivity with the groundwater table.

## 6. Conclusion

What emerges from this study is that understanding the dominant hydrologic controls governing reservoir outflow is key to improving reservoir outflow estimations. The dramatic difference in hydrologic controls between the two reservoirs used in this study indicates that the results from these reservoirs are not transferable to regions with differing climate and geography. For example, evaporation was found to have little effect on the two reservoirs studied here, but other regions such as the Middle East or a semiarid region (e.g., Lake Mead in U.S.) would have higher evaporation rates and the importance of this hydrologic control would need to be reassessed. Furthermore, reservoirs of varying sizes and functions may also behave differently in terms of hydrologic controls. As seen here, reservoirs that can store a smaller percentage of their annual inflow tend to be more dynamically operated than larger reservoirs. In more extreme cases, these reservoir dynamics may occur more often at time scales shorter than monthly. This influences which hydrologic controls are important in estimating the reservoir outflow between satellite overpasses. Additionally, the purpose of the reservoir might dictate its response to different hydrologic controls. Further work needs to be conducted to determine how reservoir size and use affects the hydrologic controls of this mass balance. This involves scaling up the method used here to multiple reservoirs of varying conditions, regulations and storage capacity. Additional studies should also examine reservoirs on a global scale to determine how well this method works in a wide variety of climates and geographies.

The success of aggregating monthly discharge estimates to generate annual estimates suggests a similar approach may be viable at shorter time scales. For example, multiple submonthly discharge estimates aggregated to generate a monthly estimate could be more accurate than the monthly estimates made here. This could be done by leveraging the power of multiple altimeters to provide more frequent storage change observations. The near future looks quite promising in terms of satellite observations of reservoir levels at higher frequencies. The currently flying AltiKa altimeter (onboard the Indian French SARAL mission) and JASON-2, and recently launched JASON-3, will be joined by Sentinel 3A and 3B (European Space Agency missions), and ICESat 2 (a laser altimeter planned for launch in 2017). The Surface Water and Ocean Topography (SWOT) mission, scheduled to launch in 2020, will provide wide-swath altimetry measurements of both water surface area and elevation, allowing for the observation of storage change without the need to derive a relationship between storage and elevation [*Pavelsky et al.*, 2014; *Biancamaria et al.*, 2015]. Thus, several years from now, a suite of 5–6 altimeters can be leveraged to provide sampling of an unprecedented number of reservoirs in large river systems.

The ability to estimate reservoir outflow using satellite remote sensing has wide reaching implications in transboundary water management. Downstream stakeholders, armed with better remotely sensed observation of upstream dam operations, can make more informed decisions about a wide array of water management issues. However, the results from this study highlight the inadequacies of this method in terms of its applicability a broader range of basins. The level of accuracy achieved here might be sufficient for some larger-scale management decisions based on the operations of a large transboundary dam, or seasonal water supply predictions, but other practices require more accurate flow predictions, such as for dynamic transboundary flood management or hydropower scheduling. From a practical standpoint, the use of more complex model to represent inflow requires more input or forcing data, which undermines the practicality and global scalability of a remote sensing approach for water management of large regulated river basins. Thus, the process complexity versus outflow accuracy becomes a decision that the water management agency has to weigh in on depending on decision making needs keeping in mind the current situation, where transboundary outflow cannot be fundamentally estimated using conventional approaches.



## Appendix A: Curve Number

The SCS CN runoff equation is:

$$Q=\left\{\begin{array}{cc} 0 & P \le I_a \\ \dfrac{(P-I_a)^2}{P-I_a+S} & P > I_a \end{array}\right\}$$

where

Q = runoff, in.; AQ6

P = rainfall, in.;

S = potential maximum soil moisture retention after runoff begins, in.;

$I_a$ = initial abstraction, in.;

$$I_a=0.2S$$

$$S=\frac{1000}{CN}-10.$$

## Appendix B: Evaporation

Evaporation of water from a reservoir was estimated using an energy balance method [*Chow et al.*, 1988],

$$E_r = \frac{1}{l_v \rho_w}(R_n - H_S - G)$$

where

$E_r$ = evaporation;

$R_n$ = net radiation;

$H_s$ = sensible heat flux;

$G$ = ground heat flux;

$\rho_w$ = density of water (997 kg/m$^3$ at 25°C);

$l_v$ = the latent heat of vaporization.

The latent heat of vaporization is a function of the mean temperature (T),

$$l_v = 2.501 \times 10^6 - 2370T$$

Neglecting sensible heat flux and ground heat flux, equation (1) become,

$$E_r = \frac{R_n}{l_v \rho_w}$$



The net radiation is calculated as the difference between the net solar radiation ($R_{ns}$) and the net longwave radiation ($R_{nl}$) [*Allen et al.*, 1998],

$$R_n = R_{ns} - R_{nl}$$

The extraterrestrial solar radiation or net solar radiation incident at the top of the atmosphere depends on the latitude and the season. This extraterrestrial radiation can be expressed as [*Allen et al.*, 1998];

$$R_a = \frac{G_{sc} d_r}{\pi}[\omega_s \sin(\varphi).\sin(\delta) + \cos(\varphi).\cos(\delta).\sin(\omega_s)]$$

where

$R_a$ = the extraterrestrial radiation;

$G_{sc}$ = the solar constant (1367 W/m$^2$);

$\varphi$ = the latitude in radian;

$\omega_s$ = sunset hour angle, where $\omega_s = arccos[-\tan(\varphi).\tan(\delta)]$;

$d_r$ = the earth-sun inverse relative distance, where $d_r = 1 + 0.033\cos\left(\frac{2\pi}{365}J\right)$;

$\delta$ = solar decimation, where $\delta = 0.409\sin\left(\frac{2\pi}{365}J - 1.39\right)$ $J$ is the Julian day.

Not all of the solar radiation incident over the atmosphere reaches the ground. A portion of this extraterrestrial radiation is obstructed by clouds. The solar radiation that reaches the ground is given by [*Allen et al.*, 1998],

$$R_s = \left(a_s + b_s \frac{n}{N}\right) R_a$$

where

$N$ = daylight hours given by $N = \frac{24}{\pi}\omega_s$;

$n$ = actual duration of sunshine in hour;

$a_s$ and $b_s$ = regression constants.

AGU Water Resources Research 10.1002/2015WR017830

If we assume the clear sky situation, then $n=N$ and,

$$R_{so}=R_s=(a_s+b_s)R_a$$

When, calibrated regression constants are unavailable,

$$R_{so}=R_s=\left(0.75+2\times10^{-5}z\right)R_a$$

where, $z$ = station height above mean sea level in m (63 m at Kaptai).

After the solar radiation reaches the ground, a portion of the radiation is reflected by the surface and the net solar radiation absorbed by the surface is,

$$R_{ns}=(1-\alpha)R_s$$

where, $\alpha$ = the surface albedo assumed to be 0.1 for the lake surface.

The earth also emits energy in form of longwave. The net longwave radiation can be approximated by [*Allen et al.*, 1998],

$$R_{nl}=\sigma\left[\frac{{T_{max}}^4+{T_{min}}^4}{2}\right]\left(0.34-0.14\sqrt{e_a}\right)\left(1.35\frac{R_s}{R_{so}}-0.35\right)$$

Assuming the sky is clear ($R_s=R_{so}$),

$$R_{nl}=\sigma\left[\frac{{T_{max}}^4+{T_{min}}^4}{2}\right]\left(0.34-0.14\sqrt{e_a}\right)$$

where

$T_{max}$ and $T_{min}$ = daily maximum and minimum temperature in kelvin;

$e_a$ = vapor pressure where $e_a=R_H * e_s$;

$R_H$ = the mean daily relative humidity (assumed 78% for Kaptai [*Mortuza et al.*, 2014]);

$e_s$ = the mean daily saturated vapor pressure.

The saturated vapor pressure is given by,

$$e^o(T)=0.6108\ exp\left[\frac{17.27\ T}{T+237.3}\right]$$

And the mean daily saturated vapor pressure is given by [*Allen et al.*, 1998],

$$e_s=\frac{e^0(T_{max})+e^0(T_{min})}{2}$$

**Acknowledgments**

This work was mainly supported by NASA WATER (NNX15AC63G). In addition, the authors acknowledge the NASA Physical Oceanography program (NN13AD97G), NASA SERVIR program (NNX12AM85AG), and NASA New Investigator Program (NNX14AI01G) for supporting this work. The Institute of Water Modeling (Bangladesh) is gratefully acknowledged for their generous support with data acquisition as well accurately conveying the real-world needs of the agency, as part of a 5 year memorandum of understanding with the University of Washington's Department of Civil and Environmental Engineering. Data pertaining to reservoir heights from radar altimeter were obtained from the AVISO ftp site maintained by CNES (French Space Agency) at ftp://avisoftp.cnes.fr. Data on discharge downstream of Hungry Horse Reservoir were obtained from USGS site at http://waterdata.usgs.gov. Discharge data downstream from Kaptai Reservoir were obtained from IWM and are available upon request by emailing Ismat Ara Pervin (iap@iwmbd.org). Meteorological data for evaporation calculation were obtained from National Climatic Data Center (NCDC) at ftp://ftp.ncdc.noaa.gov/pub/data/gsod/. Finally, all data used in this study are also available upon request by emailing fhossain@uw.edu.

## References

Alsdorf, D. E., E. Rodriguez, and D. P. Lettenmaier (2007), Measuring surface water from space, *Rev. Geophys.*, *45*, RG2002, doi:10.1029/2006RG000197.

Andreadis, K., P. Storck, and D. P. Lettenmaier (2009), Modeling snow accumulation and ablation processes in forested environments, *Water Resour. Res.*, *45*, W05429, doi:10.1029/2008WR007042.

Bakker, M. H. N. (2009), Transboundary river floods and institutional capacity, *J. Am. Water Resour. Assoc.*, *45*(3), 553–566.

Benveniste, J. (2002), ENVISAT RA-2/MWR product handbook, Issue 1.2, *Rep. PO-TN-ESR-RA-0050*, Eur. Space Agency, Frascati, Italy.

Biancamaria, S., F. Hossain, and D. P. Lettenmaier (2011), Forecasting transboundary flood with satellites, *Geophys. Res. Lett.*, *38*, L11401, doi:10.1029/2011GL047290.

Biancamaria, S., D. P. Lettenmaier, and T. M. Pavelsky (2015), The SWOT mission and its capabilities for land hydrology, *Surv. Geophys.*, *37*, 307–337, doi:10.1007/s10712-015-9346-y.

Biemans, H., I. Haddeland, P. Kabat, F. Ludwig, R. Hutjes, J. Heinke, W. Von Bloh, and D. Gerten (2011), Impact of reservoirs on river discharge and irrigation water supply during the 20th century, *Water Resour. Res.*, *47*, W03509, doi:10.1029/2009WR008929.

Birkett, C. M. (1995), The contribution of TOPEX/POSEIDON to the global monitoring of climatically sensitive lakes, *J. Geophys. Res.*, *100*, 179–204.

Birkett, C. M. (2000), Synergistic remote sensing of Lake Chad: Variability of basin inundation, *Remote Sens. Environ.*, *72*, 218–236.

Brooks, R. L. (1982), Lake elevations from satellite radar altimetry from a validation area in Canada, report, Geosci. Res. Corp. AQ7

Cherkauer, K. A., and D. P. Lettenmaier (1999), Hydrologic effects of frozen soils in the upper Mississippi River basin, *J. Geophys. Res.*, *104*, 19,599–19,610.

Cherkauer, K. A., L. C. Bowling, and D. P. Lettenmaier (2003), Variable infiltration capacity cold land process model updates, *Global Planet. Change*, *38*, 151–159.

Chow, V. T., D. R. Maidment, and L. W. Mays (1988), ''Atmospheric Water'', in *Applied Hydrology*, chap. 3, pp. 53–98, International ed., McGraw-Hill, New York.

Doll, P., K. Fiedler, and J. Zhang (2009), Global-scale analysis of river flow alterations due to water withdrawals and reservoirs, *Hydrol. Earth Syst. Sci.*, *13*, 2432–2432.

Farr, T. G., et al. (2007), The shuttle radar topography mission, *Rev. Geophys.*, *45*, RG2004, doi:10.1029/2005RG000183.

Fischer, G., F. Nachtergaele, S. Prieler, H. T. van Velthuizen, L. Verelst, and D. Wiberg (2008), *Global Agro-Ecological Zones Assessment for Agriculture (GAEZ 2008)*, Int. Inst. for Appl. Syst. Anal., Laxenburg, Austria.

Gao, H. (2015), Satellite remote sensing of large lakes and reservoirs: From elevation and area to storage, *WIREs Water*, *2*, 147–157, doi:10.1002/wat2.1065.

Gao, H., C. Birkett, and D. P. Lettenmaier (2012), Global monitoring of large reservoir storage from satellite remote sensing, *Water Resour. Res.*, *48*, W09504, doi:10.1029/2012WR012063.

Gebregiorgis, A. S., Y. Tian, C. D. Peters-Lidard, and F. Hossain (2012), Tracing hydrologic model simulation error as a function of satellite rainfall estimation bias components and land use and land cover conditions, *Water Resour. Res.*, *48*, W11509, doi:10.1029/2011WR011643.

Haddeland, I., D. P. Lettenmaier, and T. Skaugen (2006), Effects of irrigation on the water and energy balances of the Colorado and Mekong river basins, *J. Hydrol.*, *324*(1-4), 210–223, doi:10.1016/j.jhydrol.2005.09.028.

Hamlet, A. F., and D. P. Lettenmaier (1999a), Effects of climate change on hydrology and water resources in the Columbia River basin, *Am. Water Res. Assoc.*, *35*(6), 1597–1623.

Hamlet, A. F., and D. P. Lettenmaier (1999b), Columbia River streamflow forecasting based on ENSO and PDO climate signals, *J. Water Resour. Plann. Manage.*, *125*(6), 333–341.

Hawkins, R. H., R. Jiang, D. E. Woodward, A. T. Hjelmfelt, and J. A. Van Mullem (2002), Runoff curve number method: Examination of the initial abstraction ratio, in *Proceedings of the Second Federal Interagency Hydrologic Modeling Conference*, U.S. Geol. Surv. AQ8

Hong, Y., B. Adler, F. Hossain, and S. Curtis (2007), Global runoff simulation using satellite rainfall estimation and SCS-CN method, *Water Resour. Res.*, *43*, W08502, doi:10.1029/2006WR005739.

Hossain, F., A. H. M. Siddique-E-Akbor, L. Mazumder, S. M. ShahNewaz, S. Biancamaria, H. Lee, and C. K. Shum (2013), Proof of concept of an operational altimeter-based forecasting system for transboundary flow, *IEEE J. Selec. Top. Appl. Remote Sens.*, *7*(2), 587–601, doi:10.1109/JSTARS.2013.2283402.

Hossain, F., et al. (2014), A promising radar altimetry satellite system for operational flood forecasting in flood-prone Bangladesh, *IEEE Mag. Geosci. Remote Sens.*, *2*, 27–36, doi:10.1109/MGRS.2014.2345414.

Hou, Y., R. K. Kakar, S. Neeck, A. A. Azarbarzin, C. D. Kummerow, M. Kojima, R. Oki, K. Nakamura, and T. Iguchi (2014), The global precipitation measurement mission, *Bull. Am. Meteorol. Soc.*, *95*, 701–722, doi:10.1175/BAMS-D-13-00164.1.

Huffman, G. J., R. F. Adler, D. T. Bolvin, G. J. Gu, E. J. Nelkin, K. P. Bowman, Y. Hong, E. F. Stocker, and D. B. Wolff (2007), The TRMM Multisatellite Precipitation Analysis (TMPA): Quasi-global, multiyear, combined-sensor precipitation estimates at fine scales, *J. Hydrometeorol.*, *8*, 38–55. AQ9

Karmakar, S., S. M. S. Haque, and M. M. Hossain (2009), Siltation in Kaptai Reservoir of Chittagong Hill Tracts Bangladesh, *J. Indian Water Works Assoc.*, *41*(4), 275–284.

Lambin, J., et al. (2010), The OSTM/Jason-2 Mission, *Mar. Geod.*, *33*(1), doi:10.1080/01490419.2010.491030. AQ10

Lee, H., C. Shum, K.-H. Tseng, J.-Y. Guo, and C.-Y. Kuo (2011), Present-day lake level variation from Envisat altimetry over the northeastern Qinghai-Tibetan Plateau: Links with precipitation and temperature, *Terr. Atmos. Oceanic Sci.*, *22*, 169–175.

Liang, X., D. P. Lettenmaier, E. F. Wood, and S. J. Burges (1994), A simple hydrologically based model of land surface water and energy fluxes for GSMs, *J. Geophys. Res.*, *99*, 14,415-14,428.

Lohmann, D., R. Nolte-Holube, and E. Raschke (1996), A large-scale horizontal routing model to be coupled to land surface parametrization schemes, *Tellus, Ser. A*, *48*, 708–721.

Lohmann, D., E. Raschke, B. Nijssen, and D. P. Lettenmaier (1998), Regional scale hydrology: I. Formulation of the VIC-2L model coupled to a routing model, *Hydrol. Sci. J.*, *43*(1), 131–141.

Loveland, T. R., B. C. Reed, J. F. Brown, D. O. Ohlen, Z. Zhu, L. Yang, and J. W. Merchant (2000), Development of a global land cover characteristics database and IGBP DISCover from 1 km AVHRR data, *Int. J. Remote Sens.*, *21*(6-7), 1303–1330, doi:10.1080/014311600210191.

Malenovsky, Z., H. Rott, J. Cihlar, M. E. Schaepman, G. Garcia-Santos, R. Fernades, and M. Berger (2012), Sentinels for Science: Potential of Sentinel-1, -2, and -3 missions for scientific observations of ocean, cryosphere, and land, *Remote Sens. Environ.*, *120*, 91–101.

Mason, I. M., A. Harris, C. M. Birkett, W. C. Cudlip, and C. G. Rapley (1990), Remote sensing of lakes for the proxy monitoring of climatic change, in *Remote Sensing and Climate Change, Proceedings of the 16th Annual Conference of the Remote Sensing Society*, pp. 314–324, Univ. Coll. Swansea, Swansea, Wales.

Muala, E., Y. A. Mohamed, Z. Duan, and P. Zaag (2014), Estimation of reservoir discharges from Lake Nasser and Roseires Reservoir in the Nile Basin using satellite altimetry and imagery data, *Remote Sens.*, *6*(8), 7522–7545, doi:10.3390/rs6087522.

Munier, S., A. Polebitstki, C. Brown, G. Belaud, and D. P. Lettenmaier (2015), SWOT data assimilation for operational reservoir management on the upper Niger River Basin, *Water Resour. Res.*, *51*, 554–575, doi:10.1002/2014WR016157.

Pavelsky, T. M., M. T. Durand, K. M. Andreadis, R. E. Beighley, R. C. D. Paiva, G. H. Allen, and Z. F. Miller (2014), Assessing the potential global extent of SWOT river discharge observations, *J. Hydrol.*, *519*, 1516–1525.

Salami, Y. D., and F. N. Nnadi (2012), Reservoir storage variations from hydrological mass balance and satellite radar altimetry, *Int. J. Water Resour. Environ. Eng.*, *4*(6), 201–207, doi:10.5897/IJWREE11.140.

Sheffield, J., G. Goteti, and E. F. Wood (2006), Development of a 50-yr high-resolution global dataset of meteorological forcings for land surface modeling, *J. Clim.*, *19*(13), 3088–3111.

Shuttleworth, W. J. (1993), Evaporation, in *Handbook of Hydrology*, pp. 4.1–4.53, edited by D. R. Maidment, McGraw-Hill, New York.

Siddique-E-Akbor, A. H. M., F. Hossain, H. Lee, and C. K. Shum (2011), Inter-comparison study of water level estimates derived from hydrodynamic-hydrologic model and satellite altimetry for a complex deltaic environment, *Remote Sens. Environ.*, *115*, 1522–1531, doi:10.1016/j.rse.2011.02.011.

State of Montana (2011), *Hungry Horse Reservoir, Montana: Biological Impact Evaluation and Operational Constraints for a Proposed 90,000-Acre-Foot Withdrawal*. AQ11

Swenson, S., and J. Wahr (2009), Monitoring the water balance of Lake Victoria, East Africa, from space, *J. Hydrol.*, *370*(1–4), 163–176, doi:10.1016/j.jhydrol.2009.03.008.

AGU Water Resources Research 10.1002/2015WR017830


Tian, Y., and C. D. Peters-Lidard (2010), A global map of uncertainties in satellite-based precipitation measurements, *Geophys. Res. Lett.*, *37*, L24407, doi:10.1029/2010GL046008.

Todini, E. (1996), The ARNO rainfall-runoff model, *J. Hydrol.*, *175*(1–4), 339–382.

United Nations Environment Programme (2004), *Addressing Existing Dams, Issue-Based Workshop Proceedings*, 14-15 June.

United States Bureau of Reclamation (2013), *Hungry Horse Dam*, U.S. Dep. of the Inter.

United States Department of Agriculture (1986), Urban hydrology for small watersheds, *Tech. Release 55*, Natl. Resour. Conserv. Serv., Conserv. Eng. Div. AQ12

United States Department of Agriculture (2009), *Web Soil Survey*, Natl. Resour. Conserv. Serv.

Verron, J., et al. (2015), The SARAL/Altika altimetry satellite mission, *Mar. Geod.*, doi:10.1080/01490419.2014.1000471. AQ13

Vörösmarty, C. J., and D. Sahagian (2000), Anthropogenic disturbance of the terrestrial water cycle, *Bioscience*s, *50*(9), 753–765.

Vörösmarty, C. J., et al. (2010), Global threats to human water security and river biodiversity, *Nature*, *467*, 555–561, doi:10.1038/nature09440.

Ward, A. D., and S. W. Trimble (2004), *Environmental Hydrology*, CRC Press, Boca Raton, Fla.

Wenger, S. J., C. H. Luce, A. F. Hamlet, D. J. Isaak, and H. M. Neville (2010), Macroscale hydrologic modeling of ecologically relevant flow metrics, *Water Resour. Res.*, *46*, W09513, doi:10.1029/2009WR008839.

Wolf, A., J. Natharius, J. Danielson, B. Ward, and J. Pender (1999), International river basins of the world, *Int. J. Water Resour. Dev.*, *15*(4), 387–427. [Cros sRef][10.1080/07900629948682]

Wu, H., J. S. Kimball, N. Mantua, and J. Stanford (2011), Automated upscaling of river 702 networks for macroscale hydrological modeling, *Water Resour. Res.*, *47*, W03517, doi:10.1029/2009WR008871.

Zarfl, C., A. Lumsdon, J. Berlekamp, L. Tydecks, and K. Tockner (2014), A global boom in hydropower dam construction, *Aquat. Sci.*, *77*, 161–170, doi:10.1007/s00027-014-0377-0.

Zhang, J., K. Xu, Y. Yang, L. Qi, S. Hayashi, and M. Watanabe (2006), Measuring water storage fluctuations in Lake Dongting, China, by Topex/Poseidon satellite altimetry, *Environ. Monit. Assess.*, *115*, 23–37.

Zhao, R. J., Y. L. Zhang, L. R. Fang, X. R. Liu, and Q. S. Zhang (1980), The Xinanjiang model, Hydrological forecasting, in *Proceedings of the Symposium on the Application of Recent Developments in Hydrological Forecasting to the Operation of Water Resource Systems*, vol. 129, pp. 351–356, Int. Assoc. of Hydrol. Sci.

Zhou, T., B. Nijssen, H. Gao, and D. P. Lettenmaier (2015), The contribution of reservoirs to global land surface water storage variations, *J. Hydrometeorol.*, *17*, 309–325, doi:10.1175/JHM-D-15-0002.1.